Mutual Information in Coupled Double Quantum Dots

Katsuaki Tanabe*

Department of Chemical Engineering, Kyoto University, Nishikyo, Kyoto 615-8510,
Japan

*Correspondence: tanabe@cheme.kyoto-u.ac.jp

Abstract

Coupled bistate multipartite systems are extensively studied as a versatile model in
the field of information thermodynamics. As such systems are functionalized via the
interaction among the particles, mutual information is a key property in their
operation. In this study, we analyze a simple numerical model comprising a set of
coupled double quantum dots, where the disconnection of the elements is
represented by the removal of Coulomb interaction between the quantum dots. We
calculate the mutual information in the model system, as the Kullback–Leibler
divergence between the connected and disconnected status, through the probability
distribution of the electronic states from the master transition-rate equations. We
reasonably demonstrate that the increase in the strength of interaction between the
quantum dots leads to higher mutual information, owing to the larger divergence in
the probability distributions of the electronic states. Our numerical model could be
a useful basic tool for the investigations of information-driven systems.

1. Introduction

In the context of information thermodynamics [1–5], the mutual information is defined as the difference between the actual Shannon entropy of the system and that in the absence of the correlations among the random variables, and represents the intensity of inter-variable correlations [6–10]. In other words, mutual information is the divergence between the actual probability distribution and that for the independence of the variables, to quantify the reduction in uncertainty for the states of the system on making measurements. Bipartite, four-state configurations are a handy model employed for the investigations in the field of information thermodynamics [11–16]. Quantum dots [17–21], often referred to as artificial atoms, are an adopted candidate for a material component of such setups [11,22–27]. The discretized density of states in quantum dots, owing to the three-dimensional confinement of electrical carriers, enables single-electron manipulation [28–30], which may make the discussions clear in information statistical mechanics. We previously studied a coupled double quantum dot system as an autonomous information engine, calculating the steady-state entropy production rate in each component, heat and electron transfer rates via the probability distribution of the four electronic states from the master transition-rate equations, to acquire device-design principles toward the realization of corresponding practical energy converters [31]. As this system strongly relies on the interaction between the quantum dots, mutual information is a key property in the operation of information engines. In the present study, we carry out simulations to analyze the mutual information between the quantum dots, to provide a simple but practically useful model setup for numerical investigations of information-driven

systems.

2. Theory and Calculation Methods

The model setup of the present study comprises two quantum dots and three thermal/electronic reservoirs around as schematically depicted in Figure 1. Each quantum dot can contain up to one electron. One quantum dot with an electronic potential energy ε_X functions as an electronic detector by "checking" whether an electron is in the other quantum dot through capacitive interaction strength or Coulomb interaction energy U between the two quantum dots. This "detector dot" is kept at a temperature T_D and connected to thermal and electronic reservoirs, both having the same temperature T_D and an electronic potential energy μ_D. The other quantum dot with an electronic potential energy ε_Y is connected to two reservoirs through electrical leads and enables an electrical current flow. This "system dot" is kept at a temperature T_S and connected to two thermal and electronic reservoirs both at T_S with electronic potential energies μ_H and μ_L ($\mu_H > \mu_L$). It should be noted that by such a connecting configuration, this quantum-dot system realizes a non-equilibrium steady state, and is productively active, performing work in exchange for the decrease in thermal energy (the *thermoelectric engine* mode operation) or the increase in entropy (the *environmental information engine* mode operation) of the reservoirs, as living bodies [31]. The potential-energy relations among the components in the setup are schematically shown in Figure 2 for clarification. This double-quantum-dot configuration as a whole can drive electrical current between the reservoirs of μ_H and μ_L through the system dot, even

in the direction from μ_L to μ_H against the potential slope and thus generate work by properly setting the transition or tunneling rates across the interfaces between the quantum dots and reservoirs, as shown in Reference 31. Each quantum dot has an electronic state 0 or 1, where 1 and 0 mean that the dot is filled or not filled (i.e., empty) with an electron, respectively. In this way, the total electronic state (x, y) will be $(0, 0)$, $(0, 1)$, $(1, 0)$, or $(1, 1)$. For the state $(1, 1)$, the electronic potential energy in the quantum dots will increase to $\varepsilon_X + U$ and $\varepsilon_Y + U$ for the detector and system dots, respectively, due to Coulomb repulsion. We set the time resolution fine enough so that no simultaneous or diagonal jump, such as a transition from $(0, 0)$ to $(1, 1)$, is assumed in our bipartite setup.

The time evolution of the probability of the state $p(x, y)$ can be generally written as a master equation:

$$d_t p(x, y) = \sum_{x', y'} \left\{ W_{x,x'}^{y;y'} p(x', y') - W_{x',x}^{y';y} p(x, y) \right\}, \quad (1)$$

where $W_{x,x'}^{y;y'}$ is the transition rate from a state (x', y') to (x, y) and we have:

$$W_{10}^{y} = \Gamma f_y \quad (2)$$

and

$$W_{01}^{y} = \Gamma \left(1 - f_y \right) \quad (3)$$

5

for the electron transfer on the detector dot and

$$W_x^{10,\upsilon} = \Gamma_x^\upsilon f_x^\upsilon \qquad (4)$$

and

$$W_x^{01,\upsilon} = \Gamma_x^\upsilon \left(1 - f_x^\upsilon\right) \qquad (5)$$

for the system dot in this model. Note again that for the jumps, either x or y is fixed at each time step. Γ is the electronic tunneling rate between the detector dot and its reservoir. We assume the density of states in the detector-side reservoir to be uniform so that Γ is independent of y. Γ_x^υ is the tunneling rate between the system dot and its reservoirs where $\upsilon = H$ or L corresponds to the higher- or lower-potential reservoir, respectively. In contrast, we assume nonuniform profiles of the density of states in the system-side reservoirs so that Γ_x^υ depends on x. Fermi distribution functions for the detector and system dots have forms of:

$$f_y = \frac{1}{1 + \exp\left(\dfrac{\varepsilon_X + yU - \mu_D}{T_D}\right)} \qquad (6)$$

and

$$f_x^\upsilon = \frac{1}{1 + \exp\left(\dfrac{\varepsilon_Y + xU - \mu_\upsilon}{T_S}\right)}, \quad (7)$$

respectively. For simplicity, the Boltzmann constant is set to unity or absorbed into the temperatures throughout this paper. We then determine the steady-state probability distribution of $p(x, y)$ for the four electronic states through the master transition-rate equations of Equation (1).

For the disconnected model, we consider the probability distribution of the states $q(x, y)$ in the system under consideration that corresponds to $p(x, y)$ for the case $U = 0$, where the interactive information between the quantum dots is removed. Incidentally, as a consequence of $U = 0$, $q(x, y) = q(x)q(y)$ holds, where $q(x) = q(x, 0) + q(x, 1)$, $q(y) = q(0, y) + q(1, y)$. We then define the mutual information in the coupled double quantum dot system, via the Kullback–Leibler divergence, as:

$$\Phi_{MI} = D_{KL}\left\{p(x, y) \| q(x, y)\right\} = \sum_{x, y} p(x, y) \ln \frac{p(x, y)}{q(x, y)}$$

$$= p(0,0)\ln\frac{p(0,0)}{q(0,0)} + p(0,1)\ln\frac{p(0,1)}{q(0,1)} + p(1,0)\ln\frac{p(1,0)}{q(1,0)} + p(1,1)\ln\frac{p(1,1)}{q(1,1)}, \quad (8)$$

where $D_{KL}\left\{p(x, y) \| q(x, y)\right\}$ is the Kullback–Leibler divergence between the probability distributions $p(x, y)$ and $q(x, y)$.

3. Results and Discussion

Figure 3 presents a set of our calculation results for the mutual information of the coupled double quantum dot system in dependence on the capacitive interaction strength or quantum-dot Coulomb repulsion energy U for varied temperatures of the detector side T_D, for the cases $\mu_D = \varepsilon_X - U/2$ and $\mu_D = \varepsilon_X + U/2$ (adopted from Reference 31). It should be noted that, because there are too many conditional parameters to change for the numerical calculations, we intentionally provided some restrictions among the parameters in this study. It is observed for all T_D's that as U increases, the mutual information increases. This resulted trend seems reasonable in the view of the integration of information in the system; stronger interaction between the quantum dots provides a higher degree of integrated information. The mutual information is observed to be strongly dependent on T_D or the relative difference between T_S and T_D. Lower T_D provides higher mutual information for a given U. This trend can be attributed to the fact that under the fixed-T_S conditions, lower T_D and thus larger difference between T_S and T_D provides higher electron-transport selectivity, functioning towards the same directionality as larger U. With no interaction between the quantum dots, $U = 0$, the four probabilities of the states almost equivalently share the pie, $q(x, y) = 0.25$. In the large-U regime, the repulsive interaction between the quantum dots tends to eliminate $p(1, 1)$. For the condition $\mu_D = \varepsilon_X - U/2$, for larger U, $p(0, 0)$ and $p(0, 1)$ approach 0.5 while the other probabilities of the states go to zero, owing to the deep reservoir level for the detector dot and ε_Y locating in the middle of μ_H and μ_L for the system dot. This situation provides the limit of mutual information as $2 \cdot 0.5 \cdot \ln(0.5/0.25) = \ln 2 \sim 0.693$, as observed in Figure 3 (a). On the other hand, for

the condition $\mu_D = \varepsilon_X + U/2$, for larger U, $p(1, 0)$ approaches unity while the others go to zero, because of the large reservoir-to-dot potential drop for the detector dot. This situation provides the limit of mutual information as $1 \cdot \ln(1/0.25) = \ln 4 \sim 1.386$, as observed in Figure 3 (b). We adopt the condition $\mu_D = \varepsilon_X + U/2$ in the following calculations for higher mutual information.

We plot the mutual information for various tunneling rates in Figure 4. We varied the tunneling rates for the electron-flow direction against the potential differences Γ_0^H and Γ_1^L while fixing the tunneling rates in the direction down the potential slopes Γ_1^H and Γ_0^L. As seen in this set of mutual-information results, the mutual information is moderately dependent on the antisymmetric relative amplitudes of the electronic tunneling rates, i.e., that Γ_0^H and Γ_1^L are larger than Γ_1^H and Γ_0^L. This type of antisymmetry was essential for the operation of the coupled double quantum dot system as an information engine and strongly influenced the information-engine efficiency [31]. However, it is observed that this is not the case for the mutual information, and it works even for the nonsymmetric case, $\Gamma_0^H = \Gamma_0^L = \Gamma_1^H = \Gamma_1^L = 0.1$.

Here, we investigate the influence of the energy levels' relative positions among the system dot and its reservoirs. Figure 5 shows the mutual information of the coupled double quantum dot system with varied μ_H and μ_L to ε_Y, keeping $\mu_H - \mu_L$ constant. The mutual information is observed to be significantly influenced by the relative positions of the energy levels of μ_H and μ_L to ε_Y. For all of the three cases,

$p(1, 0)$ approaches to unity for larger U, which is the dominant factor for the mutual information. On the other hand, $q(1, 0)$ is smaller for higher μ_H and μ_L relative to ε_Y, owing to the dominance by $q(0, 1)$ and $q(1, 1)$, which provides higher mutual information through Equation (8). The plateau in the region $U = 1\sim2$ observed in the curve for the condition $\mu_H = 3.1$, $\mu_L = 2.9$ can be explained as follows. Figure 6 plots $p(x, y)$ in dependence on U for the condition $\mu_H = 3.1$, $\mu_L = 2.9$. As observed, the evolution of $p(0, 1)$, which is the dominant factor for the increase in the mutual information in the small-U regime, by U is damped around the region $U = 1\sim2$ because the electronic energy level $\varepsilon_Y + U$ approaches μ_H and μ_L. This situation of the relation of energy levels starts the escape of the electron from the system dot out to its reservoirs, and allows the entrance of the electron into the detector dot from its higher reservoir level, in the existence of the electronic inter-dot Coulomb repulsion by U. By contrast, the conditions $\mu_H = 0.2$, $\mu_L = 0.4$ and $\mu_H = 1.1$, $\mu_L = 0.9$ exhibit no such an intermediate plateau in the evolution of mutual information by U, as observed in Figures 3–5, because $\varepsilon_Y + U$ is always higher than μ_H and μ_L. After the point $U = 2$, where $\varepsilon_Y + U$ overlaps with μ_H and μ_L, $p(1, 0)$ steeply increases and becomes the dominant factor to recover the increase in the mutual information until reaching unity. Incidentally, it is observed in Figure 6 that after the conversion of the gradients between $p(0, 1)$ and $p(1, 0)$ around $U = 1\sim2$, as explained above, $p(1, 0)$ overtakes $p(0, 1)$ exactly at the point $U = 4$, where the electronic potential energy difference $\mu_D - \varepsilon_X$ for the detector dot equals (the middle of μ_H and μ_L) $- \varepsilon_Y$ for the system dot, and thus the absorbing driving forces into the dots are leveled.

4. Conclusions

In this study, we carried out a series of numerical simulations for the mutual information in a model coupled double quantum dot system with an artificial function to "check" the electronic state of each other via the Coulomb interaction. The evolutions of the mutual information of the system in dependence on U for various setup conditions were quantitatively analyzed in relation to the probability distributions of the electronic states. It was reasonably observed that the mutual information increases with U, because stronger interaction between the quantum dots provides a higher degree of integrated information. The mutual information of the system was observed strongly dependent on the relative temperatures of the detector and system sides owing to the influence of the electron-transport selectivity, while moderately insensitive to the antisymmetric relative amplitudes of the electronic tunneling rates. The mutual information is also found to be significantly influenced by the relative positions of the energy levels of μ_H and μ_L to ε_Y, due to the drastic turnover of the dominant electronic states. Our numerical model could be a simple but useful numerical tool for the future investigations of information-driven systems.

References

[1] Zurek, W.H. Thermodynamic cost of computation, algorithmic complexity and the information metric. *Nature* **1989**, *341*, 119–124, https://doi.org/10.1038/341119a0.

[2] Liphardt, J.; Dumont, S.; Smith, S.B.; Tinoco, I.; Bustamante, C. Equilibrium information from nonequilibrium measurements in an experimental test of Jarzynski's equality. *Science* **2002**, *296*, 1832–1835, https://doi.org/10.1126/science.1071152

[3] Toyabe, S.; Sagawa, T.; Ueda, M.; Muneyuki, E.; Sano, M. Experimental demonstration of information-to-energy conversion and validation of the generalized Jarzynski equality. *Nat. Phys.* **2010**, *6*, 988–992, https://doi.org/10.1038/NPHYS1821.

[4] del Rio, L.; Aberg, J.; Renner, R.; Dahlsten, O.; Vedral, V. The thermodynamic meaning of negative entropy. *Nature* **2011**, *474*, 61–63, https://doi.org/10.1038/nature10123.

[5] Niedenzu, W.; Mukherjee, V.; Ghosh, A.; Kofman, A.G.; Kurizki, G. Quantum engine efficiency bound beyond the second law of thermodynamics. *Nat. Commun.* **2018**, *9*, 165, https://doi.org/10.1038/s41467-017-01991-6.

[6] Kraskov, A.; Stogbauer, H.; Grassberger, P. Estimating mutual information. *Phys.*

Rev. E **2004**, *69*, 066138, https://doi.org/10.1103/PhysRevE.69.066138.

[7] Wolf, M.M.; Verstraete, F.; Hastings, M.B.; Cirac, J.I. Area laws in quantum systems: Mutual information and correlations. *Phys. Rev. Lett.* **2008**, *100*, 070502, https://doi.org/10.1103/PhysRevLett.100.070502.

[8] Horowitz, J.M.; Parrondo, J.M.R. Thermodynamic reversibility in feedback processes. *EPL* **2011**, *95*, 10005, https://doi.org/10.1209/0295-5075/95/10005.

[9] Muller, U.; Hinrichsen, H. Mutual information as a two-point correlation function in stochastic lattice models. *J. Stat. Mech.* **2013**, P04021, https://doi.org/10.1088/1742-5468/2013/04/P04021.

[10] Sriluckshmy, P.V.; Mandal, I. Critical scaling of the mutual information in two-dimensional disordered Ising models. *J. Stat. Mech.* **2018**, 043301, https://doi.org/10.1088/1742-5468/aab1b6.

[11] Schaller, G.; Kieblich, G.; Brandes, T. Low-dimensional detector model for full counting statistics: Trajectories, back action, and fidelity. *Phys. Rev. B* **2010**, *82*, 041303, https://doi.org/10.1103/PhysRevB.82.041303.

[12] Barato, A.C.; Hartich, D.; Seifert, U. Rate of mutual information between coarse-grained non-Markovian variables. *J. Stat. Phys.* **2013**, *153*, 460–478, https://doi.org/10.1007/s10955-013-0834-5.

[13] Hartich, D.; Barato, A.C.; Seifert, U. Stochastic thermodynamics of bipartite systems: Transfer entropy inequalities and a Maxwell's demon interpretation. *J. Stat. Mech.* **2014**, P02016, https://doi.org/10.1088/1742-5468/2014/02/P02016.

[14] Kutvonen, A.; Koski, J.; Ala-Nissila, T. Thermodynamics and efficiency of an autonomous on-chip Maxwell's demon. *Sci. Rep.* **2016**, *6*, 21126, https://doi.org/10.1038/srep21126.

[15] Yamamoto, S.; Ito, S.; Shiraishi, N.; Sagawa, T. Linear irreversible thermodynamics and Onsager reciprocity for information-driven engines. *Phys. Rev. E* **2016**, *94*, 052121, https://doi.org/10.1103/PhysRevE.94.052121.

[16] Horowitz, J.M.; Gingrich, T.R. Thermodynamic uncertainty relations constrain non-equilibrium fluctuations. *Nat. Phys.* **2020**, *16*, 15–20, https://doi.org/10.1038/s41567-019-0702-6.

[17] Arakawa, Y.; Sakaki, H. Multidimensional quantum well laser and temperature dependence of its threshold current. *Appl. Phys. Lett.* **1982**, *40*, 939–941, https://doi.org/10.1063/1.92959.

[18] Tessler, N.; Medvedev, V.; Kazes, M.; Kan, S.; Banin, U. Efficient near-infrared polymer nanocrystal light-emitting diodes. *Science* **2002**, *295*, 1506–1508, https://doi.org/10.1126/science.1068153.

[19] Tanabe, K.; Nomura, M.; Guimard, D.; Iwamoto, S.; Arakawa, Y. Room

temperature continuous wave operation of InAs/GaAs quantum dot photonic crystal nanocavity laser on silicon substrate. *Opt. Express* **2009**, *17*, 7036–7042, https://doi.org/10.1364/OE.17.007036.

[20] Tanabe, K.; Guimard, D.; Bordel, D.; Arakawa, Y. High-efficiency InAs/GaAs quantum dot solar cells by metalorganic chemical vapor deposition. *Appl. Phys. Lett.* **2012**, *100*, 193905, https://doi.org/10.1063/1.4714767.

[21] Bao, J.; Bawendi, M.G. A colloidal quantum dot spectrometer. *Nature* **2015**, *523*, 67–70, https://doi.org/10.1038/nature14576.

[22] Esposito, M.; Schaller, G. Stochastic thermodynamics for "Maxwell demon" feedbacks. *EPL* **2012**, *99*, 30003, https://doi.org/10.1209/0295-5075/99/30003.

[23] Strasberg, P.; Schaller, G.; Brandes, T.; Esposito, M. Thermodynamics of a physical model implementing a Maxwell demon. *Phys. Rev. Lett.* **2013**, *110*, 040601, https://doi.org/10.1103/PhysRevLett.110.040601.

[24] Horowitz, J.M.; Esposito, M. Thermodynamics with continuous information flow. *Phys. Rev. X* **2014**, *4,* 031015, https://doi.org/10.1103/10.1103/PhysRevX.4.031015.

[25] Thierschmann, H.; Sánchez, R.; Sothmann, B.; Arnold, F.; Heyn, C.; Hansen, W.; Buhmann, H.; Molenkamp, L.W. Three-terminal energy harvester with coupled quantum dots. *Nat. Nanotechnol.* **2015**, *10*, 854–858,

https://doi.org/10.1038/NNANO.2015.176.

[26] Kutvonen, A.; Sagawa, T.; Ala-Nissila, T. Thermodynamics of information exchange between two coupled quantum dots. *Phys. Rev. E* **2016**, *93*, 032147, https://doi.org/10.1103/PhysRevE.93.032147.

[27] Erdman, P.A.; Bhandari, B.; Fazio, R.; Pekola, J.P.; Taddei, F. Absorption refrigerators based on Coulomb-coupled single-electron systems. *Phys. Rev. B* **2018**, *98*, 045433, https://doi.org/10.1103/PhysRevB.98.045433.

[28] Ono, K.; Austing, D.G.; Tokura, Y.; Tarucha, S. Current rectification by Pauli exclusion in a weakly coupled double quantum dot system. *Science* **2002**, *297*, 1313–1317, https://doi.org/10.1126/science.1070958.

[29] Fujisawa, T.; Hayashi, T.; Tomita, R.; Hirayama, Y. Bidirectional counting of single electrons. *Science* **2006**, *312*, 1634–1636, https://doi.org/10.1126/science.1126788.

[30] Schaller, G.; Emary, C.; Kiesslich, G.; Brandes, T. Probing the power of an electronic Maxwell's demon: Single-electron transistor monitored by a quantum point contact. *Phys. Rev. B* **2011**, *84*, 085418, https://doi.org/10.1103/PhysRevB.84.085418.

[31] Tanabe, K. Coupled-double-quantum-dot environmental information engines: A numerical analysis. *J. Phys. Soc. Jpn.* **2016**, *85*, 064003,

Figure captions

Figure 1. Schematic illustration of the model coupled double quantum dot system.

Figure 2. Schematic diagram of the relationship among the potential energy levels in the components of the coupled double quantum dot system model setup.

Figure 3. Mutual information Φ_{MI} in the coupled double quantum dot system in dependence on the capacitive interaction strength between the quantum dots U for various temperatures of the detector quantum dot T_D for the cases (a) $\mu_D = \varepsilon_X - U/2$ and (b) $\mu_D = \varepsilon_X + U/2$ under the condition $\varepsilon_X = \varepsilon_Y = 1$, $\mu_H = 1.1$, $\mu_L = 0.9$, $T_S = 1$, $\Gamma = 100$, $\Gamma_0^H = \Gamma_1^L = 10$, and $\Gamma_1^H = \Gamma_0^L = 0.1$. QD stands for quantum dot.

Figure 4. Mutual information Φ_{MI} in dependence on the capacitive interaction strength between the quantum dots U for various tunneling rates Γ_0^H and Γ_1^L, under the condition $\varepsilon_X = \varepsilon_Y = 1$, $\mu_H = 1.1$, $\mu_L = 0.9$, $T_D = 0.1$, $T_S = 1$, $\Gamma = 100$, and $\Gamma_1^H = \Gamma_0^L = 0.1$.

Figure 5. Mutual information Φ_{MI} in dependence on the capacitive interaction strength between the quantum dots U for various relative energy-level positions μ_H and μ_L to ε_Y, keeping $\mu_H - \mu_L = 0.2$ constant, under the condition $\varepsilon_X = \varepsilon_Y = 1$, $T_D = 0.1$, $T_S = 1$, $\Gamma = 100$, $\Gamma_0^H = \Gamma_1^L = 10$, and $\Gamma_1^H = \Gamma_0^L = 0.1$.

Figure 6. Probability of the state $p(x, y)$ in the coupled double quantum dot system in dependence on the capacitive interaction strength between the quantum dots U under the condition $\varepsilon_X = \varepsilon_Y = 1$, $\mu_H = 3.1$, $\mu_L = 2.9$, $T_D = 0.1$, $T_S = 1$, $\Gamma = 100$, $\Gamma_0^H = \Gamma_1^L = 10$, and $\Gamma_1^H = \Gamma_0^L = 0.1$.
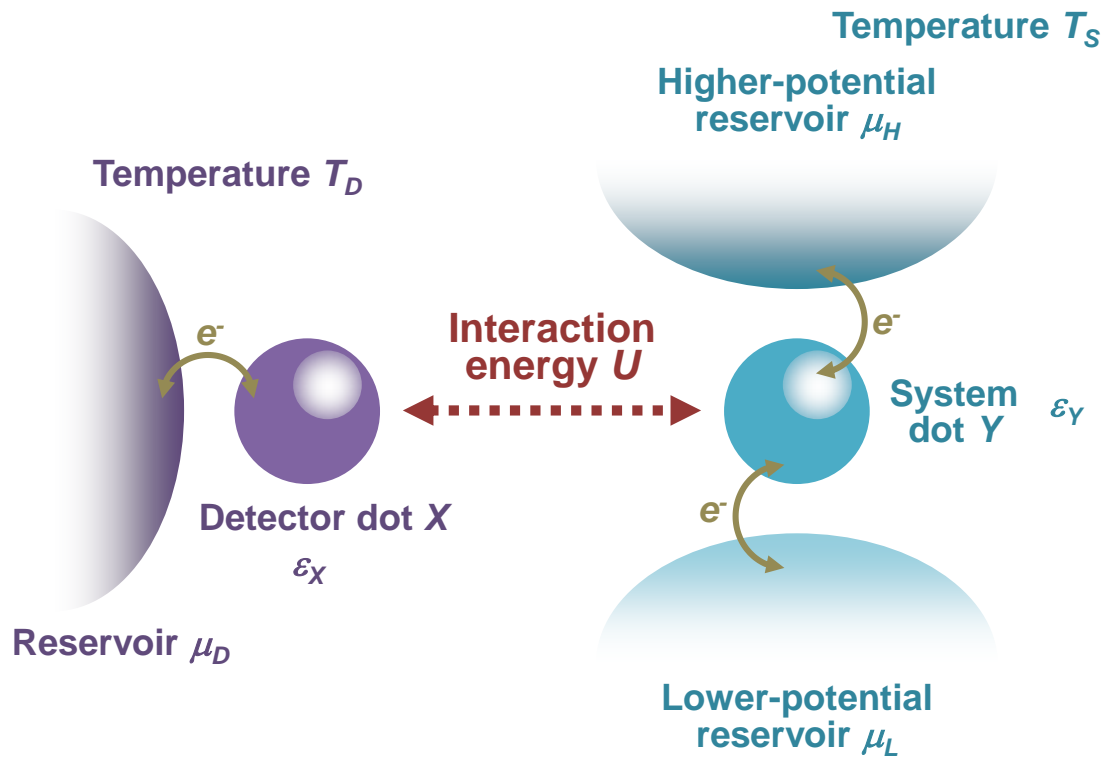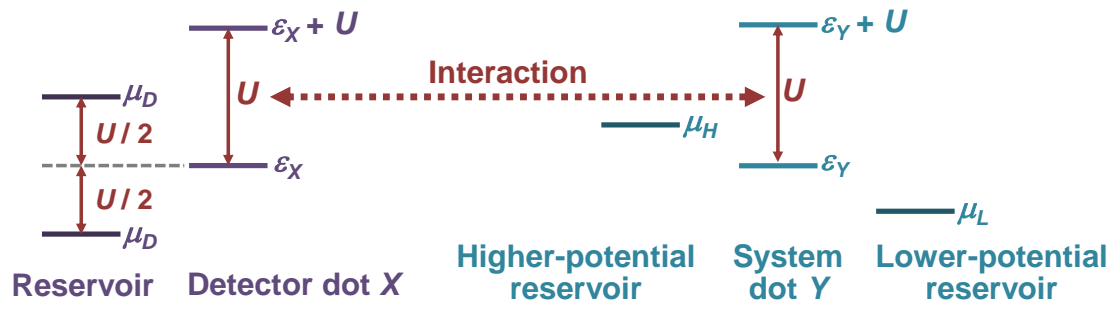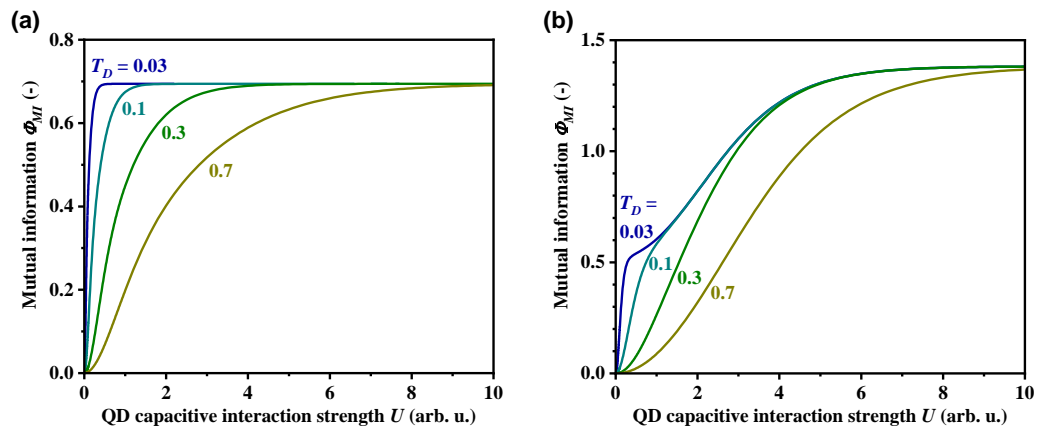
Figures

Temperature T_S

Higher-potential reservoir μ_H

Temperature T_D

Interaction energy U

e^-

e^-

System dot Y ε_Y

Detector dot X ε_X

e^-

Reservoir μ_D

Lower-potential reservoir μ_L

Figure 1

$\varepsilon_X + U$

μ_D

$U/2$

U **Interaction** U

ε_X

$U/2$

μ_D

$\varepsilon_Y + U$

μ_H

ε_Y

μ_L

Reservoir **Detector dot X** **Higher-potential reservoir** **System dot Y** **Lower-potential reservoir**

Figure 2

(a)

Mutual information Φ_{MI} (-)

$T_D = 0.03$

0.1

0.3

0.7

QD capacitive interaction strength U (arb. u.)

(b)

Mutual information Φ_{MI} (-)

$T_D =$
0.03

0.1
0.3
0.7

QD capacitive interaction strength U (arb. u.)

Figure 3

Figure 4

Figure 5

Figure 6